Chalcogenide All-solid Hybrid Microstructured Optical Fiber with Flattened Normal Dispersion and High Birefringence in the mid-IR Region

Hoang Tuan Tong, Hoa Phuoc Trung Nguyen, Takenobu Suzuki and Yasutake Ohishi
Research Center for Advanced Photon Technology, Toyota Technological Institute,
2-12-1 Hisakata, Tempaku, Nagoya, 468-8511, Japan

Keywords: Chalcogenide Microstructured Optical Fibers, Chromatic Dispersion, Birefringence Fiber, Supercontinum Generation.

Abstract: We propose in this work a new chalcogenide hybrid microstructured optical fiber with all-solid structure to realize a flattened normal chromatic dispersion profile in a broad wavelength range which is important for highly coherent and broad bandwidth supercontinuum generation in the mid-infrared window. The calculated results show that the normal dispersion regime can be obtained from 4.5 to 13 μm with the flatness of 4 ps/km-nm. In addition, the birefringence properties of the proposed fiber are investigated. The effects of breaking the symmetry of the fiber structure and increasing the refractive index difference between the core and the cladding solid rods can make the phase birefringence reach the values of the order of 10^{-3}.

1 INTRODUCTION

Mid-infrared supercontinuum (MIR SC) light sources are expected to have many potential applications, such as bio-photonic diagnostics (Verdonck, 2016), spectroscopy (Cruz, 2015) and infrared imaging (Su, 2014) due to the presence of unique molecular absorption bands in the MIR region. Among a variety of nonlinear optical fibers which have been widely studied for the generation of MIR SC, chalcogenide optical fibers have great advantages because they have wide transmission window up to around 18 μm and high nonlinearity (Kohoutek, 2013; Zakery, 2003; Romanova, 2014). Aiming at the generation of very broad SC spectral bandwidth, a great number of studies on SC generation by pumping highly nonlinear optical fibers in the anomalous dispersion regime have been demonstrated. However, the generated SC spectra are usually incoherent and the output SC pulses have complex temporal properties (Dudley, 2006). More recently, several studies showed that highly coherent SC generation could be achieved by pumping in the normal dispersion regime to overcome the low coherence and complex temporal properties (Klimczak, 2014; Liu, 2016; Klimczak, 2016), but this pumping scheme drastically reduced the SC spectral bandwidth. To maintain the high coherence and improve the spectral bandwidth of SC, a broad and flattened chromatic dispersion in the normal dispersion regime is important. In addition, to minimize detrimental effects such as, polarization mode dispersion, polarization noise and instability, polarization-maintaining chalcogenide fibers which have high birefringence are potential candidates (Caillaud, 2016; Ghosh, 2019). However, high birefringence properties were demonstrated by using photonic crystal fibers with very complex elliptical air-hole structures which are very difficult to fabricate (Dabas, 2011; Yue, 2007; Hui, 2018; Saha, 2019).

In our previous work (Nagasaka, 2017), it was shown that a broadband and highly coherent MIR SC can be generated in a chalcogenide double-clad fiber using femtosecond pulses to pump in the normal dispersion regime. The fiber was experimentally fabricated by using As_2Se_3, $AsSe_2$ and As_2S_5 chalcogenide glasses. In this work, we propose a new chalcogenide all-solid hybrid microstructured optical fiber (Ch-ASHMOF) with only one ring of 6 circular solid rods in the cladding and a high-index circular core in the center to obtain

Tong, H., Nguyen, H., Suzuki, T. and Ohishi, Y.
Chalcogenide All-solid Hybrid Microstructured Optical Fiber with Flattened Normal Dispersion and High Birefringence in the mid-IR Region.
DOI: 10.5220/0009804500930098
In *Proceedings of the 17th International Joint Conference on e-Business and Telecommunications (ICETE 2020) - DCNET, OPTICS, SIGMAP and WINSYS*, pages 93-98
ISBN: 978-989-758-445-9

a more flattened chromatic dispersion in a broad wavelength range of the normal dispersion regime. Due to the absence of complex air-hole structures, the fiber fabrication is more feasible than using complex elliptical air-hole structures. The results show that flattened chromatic dispersion can be obtained from 4.5 to 13 µm with the flatness of 4 ps/km-nm. In addition, the birefringence properties of the fiber are investigated by tuning the geometrical parameters and increasing the refractive index difference between the core and cladding rods. As a result, the phase birefringence can reach the values of the order of 10^{-3}.

2 MATERIAL PROPERTIES

Figure 1a shows the refractive index profiles of As_2Se_3, $AsSe_2$ and As_2S_5 chalcogenide glasses. They were measured by using ellipsometry method. The refractive index difference between As_2Se_3 and As_2S_5 is as large as 0.6 whereas refractive indices of As_2Se_3 and $AsSe_2$ are close. Based on the measured refractive index data in Fig. 1a, the material dispersions of those glasses were calculated and are shown in Fig. 1b. The zero-dispersion wavelengths of As_2Se_3, $AsSe_2$ and As_2S_5 glasses were 6.5, 7.2 and 5.2 µm, respectively. The material dispersion of As_2S_5 rapidly increases beyond 5 µm but material dispersions of As_2Se_3 and $AsSe_2$ gradually increase beyond 6 µm. In Fig. 1c, transmission spectra of As_2Se_3, $AsSe_2$ and As_2S_5 glasses are shown. The transmission spectra were measured using a UV/VIS/NIR spectrometer (Perkin Elmer, Lambda 900) and an FTIR spectrometer (Perkin Elmer, Spectrum 100) with 1 mm-thick samples. As_2Se_3 and $AsSe_2$ glasses are still transparent (higher than 40%) beyond 13 µm, whereas As_2S_5 glass is not transparent over 13 µm. An absorption band above 9 µm of As_2S_5 glass is caused by the As-S bonds. Absorption bands from 14 to 16 µm and above 17 µm of As_2Se_3 and $AsSe_2$ glasses are caused by the As-Se bonds. An absorption peak at 12 µm which is caused by the Se-OH bonds is found only for $AsSe_2$.

3 FIBER DESIGN

3.1 Flattened Chromatic Dispersion

In our previous work (Nagasaka, 2017), we demonstrated a chalcogenide double cladding fiber

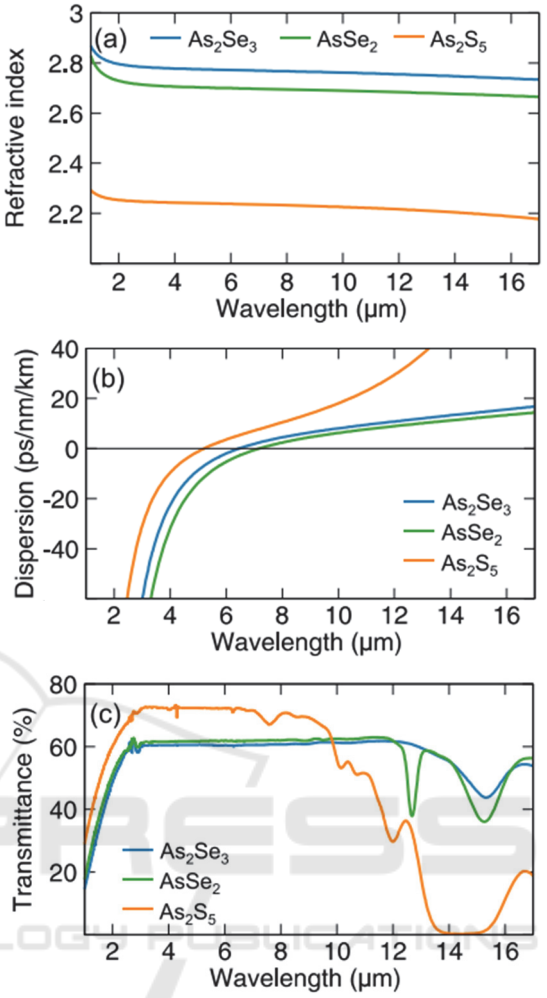

Figure 1: (a) Refractive index, (b) material dispersion and (c) transmission properties of As_2Se_3, $AsSe_2$ and As_2S_5 chalcogenide glasses, respectively.

(Ch-DCF) whose core, first cladding and second cladding layers were made of the As_2Se_3, $AsSe_2$ and As_2S_5 glasses, respectively, The diameters of the core and first cladding were D_{core} = 7.8 µm and D_{clad1} = 30.7 µm, respectively. Its schematic cross-section image is shown in Fig. 2 and its calculated chromatic dispersion profile is shown in Fig. 3. A normal dispersion regime is obtained from 4.5 to 12.5 µm with a minimum of -12.5 ps/km-nm at 9.4 µm and anomalous chromatic dispersion is realized beyond 12.5 µm. Using 2.8-cm-long section of this fiber, we demonstrated SC generation extending from 2 to 14 µm at the -40 dB level by using the pump wavelength of 10 µm and the coupled pump peak power of 1.3 MW (Nagasaka, 2017).

To make the normal dispersion profile more flattened, a Ch-ASHMOF with an As_2Se_3 core, $AsSe_2$ cladding and a ring of 6 As_2S_5 rods is

proposed in this work. The diameters of the core, solid rods and pitch are D_{core}=8.0, d=1.9 and Λ=13 µm, respectively, as shown in Fig. 2. Using this Ch-ASHMOF, a normal dispersion regime whose flatness is approximately 4 ps/km-nm can be obtained from 4.5 to 13 µm as calculated and shown in Fig. 3.

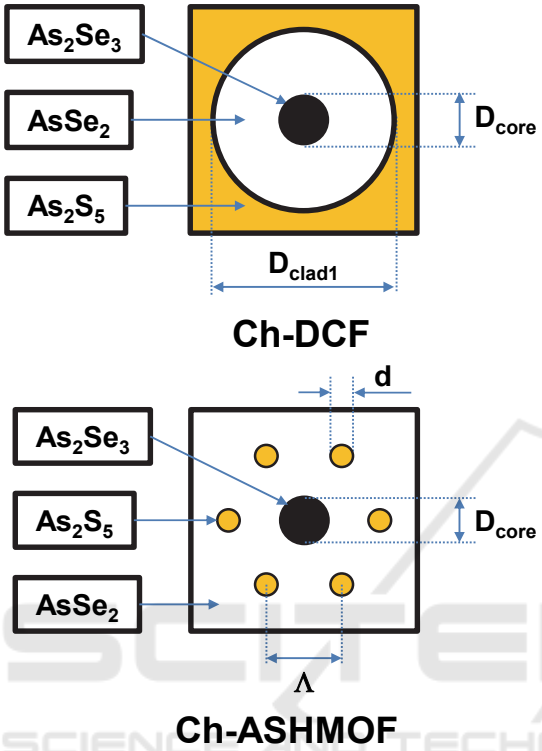

Figure 2: Schematic cross-sectional images of chalcogenide double-clad fiber (Ch-DCF) and chalcogenide all-solid hybrid microstructured optical fiber (Ch-ASHMOF).

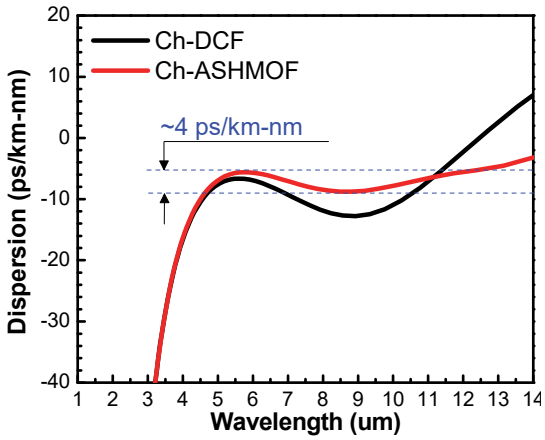

Figure 3: Calculated chromatic dispersion profiles of the Ch-DCF and Ch-ASHMOF which are depicted in Fig. 2. The calculations of chromatic dispersion profile were performed by using a commercial software (Mode Solution) from the Lumerical company.

3.2 Birefringence Properties

The phase birefringence $B(\lambda)$ is defined as the difference between n_x and n_y which are the real part of the effective refractive indices of x-polarized fundamental modes HE_{11} (slow axis) and y-polarized fundamental modes HE_{11} (fast axis) (Caillaud, 2016; Ghosh, 2019). It is calculated by using Eq. 1

$$B(\lambda) = \left| n_x(\lambda) - n_y(\lambda) \right| \quad (1)$$

Therefore, the key point of realizing the birefringence is to destroy the symmetry of fiber structure and increase the effective index difference between the two orthogonal polarization modes (Dabas, 2011). For microstructured optical fibers, high birefringence can be achieved by designing an asymmetric arrangement of air holes, not only by altering the air holes size near the core area (Caillaud, 2016; Ortigosa, 2000; Ju, 2003), but also by changing the shape of air holes (Yue, 2007), or by introducing mechanical stress as demonstrated in (Schreiber, 2005). In our work, the symmetry of the solid-rod structure is broken by modifying the properties of the L and R rods which take the core as a reflecting point as shown in Fig. 4.

Figure 4 shows the geometrical changes in the cross-sectional structures of the Ch-ASHMOFs from S0 to S1, S2a and S3a. In fact, the changes occur only for the L and R rods whereas other components keep constant. In S1 and S3a, the diameters of the L and R rods increase from 1.9 to 4 and 8 µm, respectively, as compared to that in S0. Furthermore, in S2a, the distances from the core to the centers of

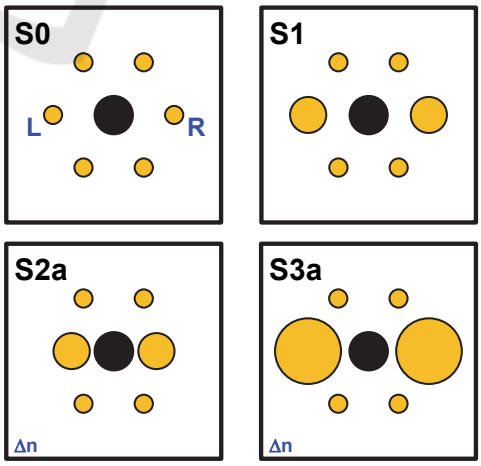

Figure 4: Schematic cross-sectional images of Ch-ASHMOFs (S0, S1, S2a and S3a). The two As_2S_5 (L and R) rods in these structures were modified to study their effects on the phase birefringence of the fiber.

the L and R rods become shorter and the diameters of the L and R rods are 4 μm.

The calculated wavelength dependence of the phase birefringence profiles corresponding to S0, S1, S2a and S3a fiber structures are shown in Fig. 5. It can be noticed that the phase birefringence increases significantly as depicted by the red line (S2a) when the L and R rods get closer to the core because the symmetry of the fiber structure is strongly destroyed. Besides, the phase birefringence can be very high as shown by the blue line (S3a) when the diameters of the L and R rods become very different from the other As_2S_5 rods. As a result, the phase birefringence can reach 3.6 x10^{-3} at 12 μm.

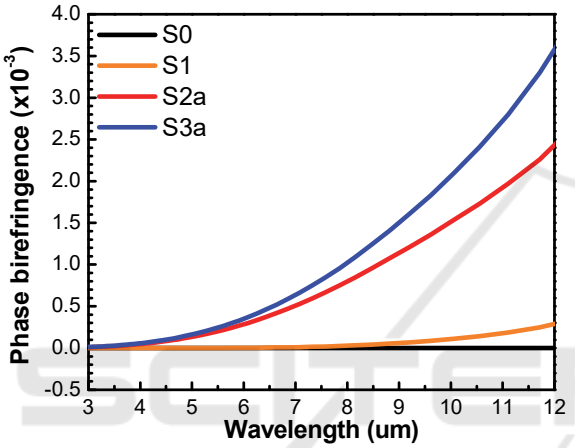

Figure 5: Calculated phase birefringence of Ch-ASHMOFs (S0, S1, S2a and S3a) whose cross-section structures were depicted in Fig. 4, respectively.

To further increase the phase birefringence, we investigate the effect of increasing the refractive index difference (Δn) between the core and the solid rods in the cladding. Figure 6 illustrates the schematic cross-sectional images of S2a, S2b and S2c structures. These structures have an identical geometry, but the refractive index of the solid rods in the cladding is assumed to be different from that of S2a, S2b and S2c. The small-grid pattern in S2b indicates that the refractive index of the solid rods in the cladding of S2b decreases by 0.05 as compared to that of the As_2S_5 in S2a. The large-grid pattern in S2c indicates that the refractive index of the solid rods in the cladding of S2c decreases by 0.1 as compared to that of the As_2S_5 in S2a. In other words, the Δn increases by 0.05 and 0.1 in S2b and S2c as compared to S2a, respectively. The calculated wavelength dependence of the phase birefringence profiles corresponding to S2a, S2b and S2c fiber structures are shown in Fig. 7 as the red solid line, dashed line and dotted line, respectively. It is obvious that the phase birefringence increases when Δn increases, especially at wavelengths longer than 7 μm.

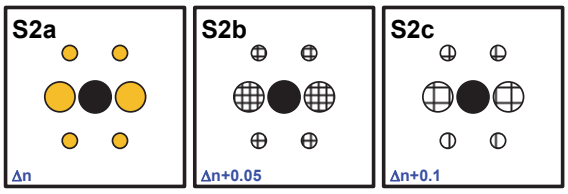

Figure 6: Schematic cross-sectional images of Ch-ASHMOFs (S2a, S2b and S2c). The refractive indices of 6 rods in the cladding of the S2b and S2c structures were assumed to decrease by 0.05 and 0.1, respectively, as compared to the measured refractive index of As_2S_5 glass which was used in the S2a structure.

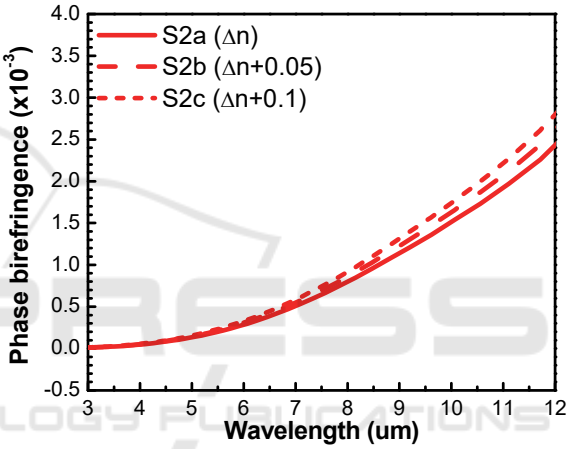

Figure 7: Calculated phase birefringence of Ch-ASHMOFs (S2a, S2b and S2c) whose cross-section structures were depicted in Fig. 6.

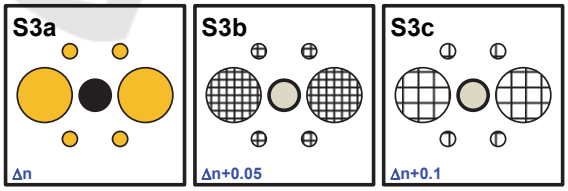

Figure 8: Schematic cross-sectional images of Ch-ASHMOFs (S3a, S3b and S3c). The refractive indices of 6 rods in the cladding of the S3b and S3c structures were assumed to decrease by 0.05 and 0.1, respectively, as compared to the measured refractive index of As_2S_5 glass which was used in the S3a structure.

Similarly, the effect of increasing Δn was investigated for the S3a fiber structure. The change in refractive index of the rods in the cladding is indicated by the small and large grid patterns in Fig. 8. The calculated wavelength dependence of

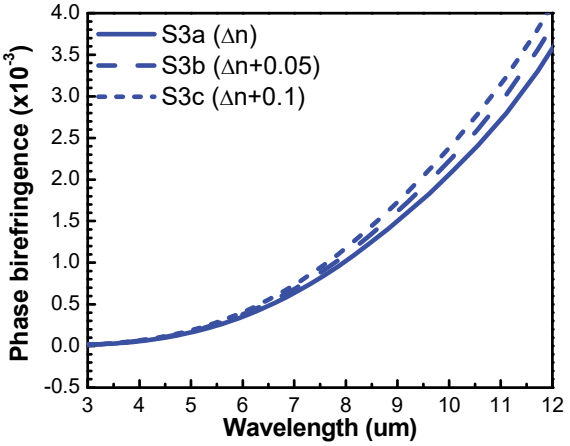

Figure 9: Calculated phase birefringence of Ch-ASHMOFs (S3a, S3b and S3c) whose cross-section structures were depicted in Fig. 8.

the phase birefringence profiles corresponding to the S3a, S3b and S3c fiber structures are shown in Fig. 9 as the blue solid line, dashed line and dotted line, respectively. As can be seen, the phase birefringence can be larger than 4.0×10^{-3} in case of the S3c structure.

4 CONCLUSIONS

In this work, a new Ch-ASHMOF made of As_2Se_3, $AsSe_2$ and As_2S_5 glasses with all-solid structure was proposed to realize a flattened chromatic dispersion in a broad wavelength range of the normal dispersion regime. The calculated results show that the normal dispersion regime can be obtained from 4.5 to 13 µm with the flatness of 4 ps/km-nm. In addition, the birefringence properties of the fiber were investigated by changing the diameter of two solid rods in the cladding to break the symmetry of the fiber structure and by increasing the refractive index difference between the core and the rods in the cladding. The combination of these effects can make the phase birefringence reach the values of the order of 10^{-3}. Due to the feasible fabrication process, flattened chromatic dispersion and the ability of controlling phase birefringence, the proposed Ch-ASHMOF can be a good candidate to realize MIR SC generation with broad bandwidth and high coherence for many potential applications.

ACKNOWLEDGEMENTS

This work was supported by the Japan Society for the Promotion of Science (JSPS) KAKENHI (Grant Number 15H02250, 17K18891 and 18H01504).

REFERENCES

Verdonck, M., Denayer, A., Delvaux, B., Garaud, S., De, W. R., Desmedt, C., Sotiriou, C., Willard, G. K. and Goormaghtigh, E., 2016. Characterization of human breast cancer tissues by infrared imaging, *Analyst*, 141, 606-619.

Cruz, F. C., Maser, D. L., Johnson, T., Ycas, G., Klose, A., Giorgetta, F. R., Coddington, I. and Diddams, S. A., 2015. Mid infrared optical frequency combs based on difference frequency generation for molecular spectroscopy, *Opt. Express*, 23, 26814-26824.

Su, R., Kirillin, M., Chang, E. W., Sergeeva, E., Yun, S. H. and Mattsson, L., 2014. Perspectives of mid-infrared optical coherence tomography for inspection and micro metrology of industrial ceramics, *Opt. Express*, 22. 15804-15819.

Kohoutek, T., Orava, J., Greer, A. L. and Fudouzi, H., 2013. Submicrometer soft lithography of a bulk chalcogenide glass, *Opt. Express*, 21, 9584-9591.

Zakery, A. and Elliott, S. R., 2003. Optical properties and applications of chalcogenide glasses: a review, *J. Non-Cryst. Solids*, 330, 1–12.

Romanova, E. A., Kuzyutkina, Y. S., Konyukhov, A. I., Abdel M. N., Seddon, A. B., Benson, T. M., Guizard, S. and Mouskeftaras, A., 2014. Nonlinear optical response and heating of chalcogenide glasses upon irradiation by the ultrashort laser pulses, *Opt. Eng.*, 53, 071812.

Dudley, J. M., Genty, G. and Coen, S., 2006. Supercontinuum generation in photonic crystal fiber, *Rev. Mod. Phys.*, 78, 1135–84.

Klimczak, M., Siwicki, B., Skibinski, P., Pysz, D., Stępien, R., Heidt, A., Radzewicz, C. and Buczynski, R., 2014. Coherent supercontinuum generation up to 2.3 µm in all-solid softglass photonic crystal fibers with flat all-normal dispersion, *Opt. Express*, 22, 18824-18832.

Liu, L., Cheng, T., Nagasaka, K., Tong, H.T., Qin, G., Suzuki, T. and Ohishi, Y., 2016. Coherent mid-infrared supercontinuum generation in all-solid chalcogenide microstructured fibers with all-normal dispersion, *Opt. Lett.*, 41, 392-395.

Klimczak, M., Siwicki, B., Zhou, B., Bache, M., Pysz, D., Bang, O. and Buczynski, R., 2016. Coherent supercontinuum bandwidth limitations under femtosecond pumping at 2 µm in all-solid soft glass photonic crystal fibers, *Opt. Express*, 24, 29406-29416.

Caillaud, C., Gilles, C., Provino, L., Brilland, L., Jouan, T., Ferre, S. and Troles, J., 2016. Highly birefringent chalcogenide optical fiber for polarization-maintaining in the 3-8.5 µm mid-IR window, *Opt. Express*, *24*, 7977-7986.

Ghosh, A. N., Meneghetti, M., Petersen, C. R., Bang, O.,

Brilland, L., Venck, S. and Sylvestre, T., 2019. Chalcogenide-glass polarization-maintaining photonic crystal fiber for mid-infrared supercontinuum generation, *J. Phys. Photonics*, *1*, 044003.

Dabas, B. and Sinha, R. K., 2011. Design of highly birefringent chalcogenide glass PCF: A simplest design, *Opt. Commun.*, 284, 1186-1191.

Yue, Y., Kai, G., Wang, Z., Sun, T., Jin, L., Lu, Y. and Yuan, S., 2007. Highly birefringent elliptical-hole photonic crystal fiber with squeezed hexagonal lattice, *Opt. Lett.*, *32*(5), 469-471.

Hui, Z., Yang, M., Zhang, Y. and Zhang, M., 2018. Mid-infrared high birefringence As2Se3-based PCF with large nonlinearity and distinctive dispersion by using asymmetric elliptical air hole cladding, *Mod. Phys. Lett. B*, 32, 1850023.

Saha, R., Hossain, M.M., Rahaman, M.E. and Mondal, H.S., 2019. Design and analysis of high birefringence and nonlinearity with small confinement loss photonic crystal fiber, *Front. Optoelectron*., *12*, 165-173.

Nagasaka, K., Liu, L., Tuan, T. H., Cheng, T., Matsumoto, M., Tezuka, H., Suzuki, T. and Ohishi, Y., 2017. Supercontinuum generation in chalcogenide double-clad fiber with near zero-flattened normal dispersion profile. *J. Opt*, 19, 095502.

Ortigosa, B. A., Knight, J. C., Wadsworth, W. J., Arriaga, J., Mangan, B. J., Birks, T. A. and Russell, P. S. J., 2000. Highly birefringent photonic crystal fibers, *Opt. Lett.*, 25, 1325-1327.

Ju, J., Jin, W. and Demokan, M. S., 2003. Properties of a highly birefringent photonic crystal fiber, *IEEE Photon. Technol. Lett.,* 15, 1375-1377.

Yue, Y., Kai, G., Wang, Z., Sun, T., Jin, L., Lu, Y., Zhang, C., Liu, J., Li, Y., Liu, Y. and Yuan, S., 2007. Highly birefringent elliptical-hole photonic crystal fiber with squeezed hexagonal lattice, *Opt. Lett.*, 32, 469-471.

Schreiber, T., Röser, F., Schmidt, O., Limpert, J., Iliew, R., Lederer, F., Petersson, A., Jacobsen, C., Hansen, K.P., Broeng, J. and Tünnermann, A., 2005. Stress-induced single-polarization single-transverse mode photonic crystal fiber with low nonlinearity, *Opt. Express*, 13, 7621-7630.